Measurement of the $N \to \Delta^+(1232)$ Transition at High Momentum Transfer by π^0 Electroproduction

M. Ungaro,[1,2,3] P. Stoler,[1] I. Aznauryan,[3,40] V.D. Burkert,[3] K. Joo,[2] L.C. Smith,[38] G. Adams,[1] M. Amarian,[31] P. Ambrozewicz,[13] M. Anghinolfi,[19] G. Asryan,[40] G. Audit,[9] H. Avakian,[3] H. Bagdasaryan,[40,31] J.P. Ball,[4] N.A. Baltzell,[35] S. Barrow,[14] V. Batourine,[24] M. Battaglieri,[19] I. Bedliski,[22] M. Bektasoglu,[31,30] M. Bellis,[1,7] N. Benmouna,[15] B.L. Berman,[15] A.S. Biselli,[1,7] B.E. Bonner,[33] S. Bouchigny,[20] S. Boiarinov,[22,3] R. Bradford,[7] D. Branford,[11] W.J. Briscoe,[15] W.K. Brooks,[3] S. Bültmann,[31] C. Butuceanu,[39] J.R. Calarco,[28] S.L. Careccia,[31] D.S. Carman,[30] A. Cazes,[35] S. Chen,[14] P.L. Cole,[3,8,17] P. Coltharp,[14] D. Cords,[3] P. Corvisiero,[19] D. Crabb,[38] J.P. Cummings,[1] E. De Sanctis,[18] R. DeVita,[19] P.V. Degtyarenko,[3] H. Denizli,[32] L. Dennis,[14] A. Deur,[3] K.V. Dharmawardane,[31] C. Djalali,[35] G.E. Dodge,[31] J. Donnelly,[16] D. Doughty,[10,3] M. Dugger,[4] S. Dytman,[32] O.P. Dzyubak,[35] H. Egiyan,[39,3] K.S. Egiyan,[40] L. Elouadrhiri,[3] P. Eugenio,[14] R. Fatemi,[38] G. Fedotov,[27] G. Feldman,[15] R.J. Feuerbach,[7] H. Funsten,[39] M. Garçon,[9] G. Gavalian,[28,31] G.P. Gilfoyle,[34] K.L. Giovanetti,[23] F.X. Girod,[9] J. Goetz,[5] C.I.O. Gordon,[16] R.W. Gothe,[35] K.A. Griffioen,[39] M. Guidal,[20] M. Guillo,[35] N. Guler,[31] L. Guo,[3] V. Gyurjyan,[3] C. Hadjidakis,[20] R.S. Hakobyan,[8] J. Hardie,[10,3] D. Heddle,[3] F.W. Hersman,[28] I. Hleiqawi,[30] M. Holtrop,[28] K. Hicks,[30] C.E. Hyde-Wright,[31] Y. Ilieva,[15] D.G. Ireland,[16] B.S. Ishkhanov,[27] M.M. Ito,[3] D. Jenkins,[37] H.S. Jo,[20] H.G. Juengst,[15,31] J.D. Kellie,[16] M. Khandaker,[29] W. Kim,[24] A. Klein,[31] F.J. Klein,[8] A.V. Klimenko,[31] M. Kossov,[22] L.H. Kramer,[13,3] V. Kubarovsky,[1] J. Kuhn,[1,7] S.E. Kuhn,[31] J. Lachniet,[7,31] J.M. Laget,[3] J. Langheinrich,[35] D. Lawrence,[26] T. Lee,[28] Ji Li,[1] K. Livingston,[16] C. Marchand,[9] N. Markov,[2] S. McAleer,[14] B. McKinnon,[16] J.W.C. McNabb,[7] B.A. Mecking,[3] S. Mehrabyan,[32] J.J. Melone,[16] M.D. Mestayer,[3] C.A. Meyer,[7] K. Mikhailov,[22] R. Minehart,[38] M. Mirazita,[18] R. Miskimen,[26] V. Mokeev,[27] L. Morand,[9] S.A. Morrow,[20,9] J. Mueller,[32] G.S. Mutchler,[33] J. Napolitano,[1] R. Nasseripour,[13] S. Niccolai,[15,20] G. Niculescu,[30,23] I. Niculescu,[15,3,23] B.B. Niczyporuk,[3] M. Niroula,[31] R.A. Niyazov,[31,3] M. Nozar,[3] G.V. O'Rielly,[15] M. Osipenko,[19,27] A.I. Ostrovidov,[14] K. Park,[24] E. Pasyuk,[4] S.A. Philips,[15] N. Pivnyuk,[22] D. Pocanic,[38] O. Pogorelko,[22] E. Polli,[18] S. Pozdniakov,[22] B.M. Preedom,[35] J.W. Price,[6] Y. Prok,[38,3,*] D. Protopopescu,[28,16] L.M. Qin,[31] B.A. Raue,[13,3] G. Riccardi,[14] G. Ricco,[19] M. Ripani,[19] B.G. Ritchie,[4] F. Ronchetti,[18] G. Rosner,[16] P. Rossi,[18] P.D. Rubin,[34] F. Sabatié,[9] C. Salgado,[29] J.P. Santoro,[37,3,8] V. Sapunenko,[3] R.A. Schumacher,[7] V.S. Serov,[22] Y.G. Sharabian,[3] A.V. Skabelin,[25] E.S. Smith,[3] D.I. Sober,[8] A. Stavinsky,[22] S.S. Stepanyan,[24] S. Stepanyan,[10,3] B.E. Stokes,[14] I.I. Strakovsky,[15] S. Strauch,[15,35] M. Taiuti,[19] D.J. Tedeschi,[35] U. Thoma,[3,21,12,†] A. Tkabladze,[30,15] L. Todor,[7,34] S. Tkachenko,[31] C. Tur,[35] M.F. Vineyard,[36,34] A.V. Vlassov,[22] L.B. Weinstein,[31] D.P. Weygand,[3] M. Williams,[7] E. Wolin,[3] M.H. Wood,[35,‡] A. Yegneswaran,[3] L. Zana,[28] B. Zhang,[25] J. Zhang,[31] and B. Zhao[2]

(The CLAS Collaboration)

[1] *Rensselaer Polytechnic Institute, Troy, New York 12180-3590*
[2] *University of Connecticut, Storrs, Connecticut 06269*
[3] *Thomas Jefferson National Accelerator Facility, Newport News, Virginia 23606*
[4] *Arizona State University, Tempe, Arizona 85287-1504*
[5] *University of California at Los Angeles, Los Angeles, California 90095-1547*
[6] *California State University, Dominguez Hills, Carson, CA 90747*
[7] *Carnegie Mellon University, Pittsburgh, Pennsylvania 15213*
[8] *Catholic University of America, Washington, D.C. 20064*
[9] *CEA-Saclay, Service de Physique Nucléaire, F91191 Gif-sur-Yvette,Cedex, France*
[10] *Christopher Newport University, Newport News, Virginia 23606*
[11] *Edinburgh University, Edinburgh EH9 3JZ, United Kingdom*
[12] *Emmy-Noether Foundation, Germany*
[13] *Florida International University, Miami, Florida 33199*
[14] *Florida State University, Tallahassee, Florida 32306*
[15] *The George Washington University, Washington, DC 20052*
[16] *University of Glasgow, Glasgow G12 8QQ, United Kingdom*
[17] *Idaho State University, Pocatello, Idaho 83209*
[18] *INFN, Laboratori Nazionali di Frascati, 00044 Frascati, Italy*
[19] *INFN, Sezione di Genova, 16146 Genova, Italy*
[20] *Institut de Physique Nucleaire ORSAY, Orsay, France*
[21] *Institute für Strahlen und Kernphysik, Universität Bonn, Germany*
[22] *Institute of Theoretical and Experimental Physics, Moscow, 117259, Russia*
[23] *James Madison University, Harrisonburg, Virginia 22807*

[24] Kyungpook National University, Daegu 702-701, South Korea
[25] Massachusetts Institute of Technology, Cambridge, Massachusetts 02139-4307
[26] University of Massachusetts, Amherst, Massachusetts 01003
[27] Moscow State University, General Nuclear Physics Institute, 119899 Moscow, Russia
[28] University of New Hampshire, Durham, New Hampshire 03824-3568
[29] Norfolk State University, Norfolk, Virginia 23504
[30] Ohio University, Athens, Ohio 45701
[31] Old Dominion University, Norfolk, Virginia 23529
[32] University of Pittsburgh, Pittsburgh, Pennsylvania 15260
[33] Rice University, Houston, Texas 77005-1892
[34] University of Richmond, Richmond, Virginia 23173
[35] University of South Carolina, Columbia, South Carolina 29208
[36] Union College, Schenectady, NY 12308
[37] Virginia Polytechnic Institute and State University, Blacksburg, Virginia 24061-0435
[38] University of Virginia, Charlottesville, Virginia 22901
[39] College of William and Mary, Williamsburg, Virginia 23187-8795
[40] Yerevan Physics Institute, 375036 Yerevan, Armenia[§]

We report a new measurement of the exclusive electroproduction reaction $\gamma^* p \rightarrow \pi^0 p$ to explore the evolution from soft non-perturbative physics to hard processes via the Q^2 dependence of the magnetic (M_{1+}), electric (E_{1+}) and scalar (S_{1+}) multipoles in the $N \rightarrow \Delta$ transition. 9000 differential cross section data points cover W from threshold to 1.4 GeV/c^2, 4π center-of-mass solid angle, and Q^2 from 3 to 6 GeV^2/c^2, the highest yet achieved. It is found that the magnetic form factor G_M^* decreases with Q^2 more steeply than the proton magnetic form factor, the ratio E_{1+}/M_{1+} is small and negative, indicating strong helicity non-conservation, and the ratio S_{1+}/M_{1+} is negative, while its magnitude increases with Q^2.

The $\Delta(1232)$ resonance is the lowest and most prominent baryon excitation, and the $N \rightarrow \Delta$ transition has served as a prototype for testing theoretical models of baryon structure. For electromagnetic excitations in which the Δ decays into a pion and nucleon, the transition amplitudes are expressed in terms of multipoles, which for the $N \rightarrow \Delta$ transition are the magnetic M_{1+}, electric E_{1+}, and scalar S_{1+} [1]. Alternatively, the $N \rightarrow \Delta$ transition is expressed in terms of form factors G_M^*, G_E^* and G_C^* [2].

The Q^2 dependence of the electromagnetic multipoles in the $N \rightarrow \Delta$ transition is sensitive to the evolution from soft non-perturbative physics to hard processes and perturbative QCD. At low Q^2, the small quadrupole deformation of the nucleon was long ago understood in the framework of the quark model, assuming the reaction is dominated by a single spin-flip of a constituent quark in a nearly spherical potential where M_{1+} is dominant [3, 4]. The coupling of the pion cloud to the quark core and two body exchange currents may also contribute to the small values of the E_{1+} and scalar S_{1+} multipoles [5, 6]. At high Q^2, helicity conservation in pQCD requires $E_{1+} = M_{1+}$.

This Letter presents the results of a Jefferson Lab (JLab) experiment that extends the measurement of the electromagnetic $N \rightarrow \Delta$ transition to the highest momentum transfer yet achieved, in order to explore the transition region between these low and high Q^2 regimes. The unpolarized differential cross section for exclusive π^0 electroproduction has been obtained in the hadronic mass W from threshold to 1.4 GeV/c^2, in four-momentum transfer Q^2 from 3 to 6 GeV^2/c^2, and solid angle 4π in the center of mass. The quantities G_M^*, $R_{EM} \equiv Re(E_{1+}/M_{1+})$ and $R_{SM} \equiv Re(S_{1+}/M_{1+})$, have been extracted from the measured cross sections using a unitary isobar model [7] that takes into account all available data for the Δ and higher W resonances from JLab and other laboratories.

In the one-photon-exchange approximation, the fourfold differential cross section of π^0 electroproduction can be factorized as

$$\frac{d^4\sigma}{dW\,dQ^2\,d\Omega_\pi^*} = \Gamma_v \frac{d^2\sigma}{d\Omega_\pi^*},$$

where Γ_v is the virtual photon flux and $d^2\sigma/d\Omega_\pi^*$ is the center-of-mass differential cross section for π production by a virtual photon.

For the present experiment, an electron beam of energy of 5.75 GeV was incident on a 5.0-cm-long liquid hydrogen target. The CEBAF Large Acceptance Spectrometer CLAS [8] was used to detect the scattered electrons and final state protons. Electrons were selected by a hardware trigger formed from the coincidence of signals from a threshold gas Čerenkov detector and an electromagnetic calorimeter. Multiwire drift chambers were used to reconstruct momenta by measuring particle tracks in the CLAS toroidal magnetic field. Plastic scintillators were used to record particle time of flight from the interaction point to the scintillators. From their known track length, particle velocities were computed and masses calculated using the measured momenta. Software analysis included geometrical and kinematic cuts to eliminate inefficient areas within the spectrometer. Backgrounds coming from π^-/e^- contamination were suppressed using the energy response in the calorimeter and the sig-

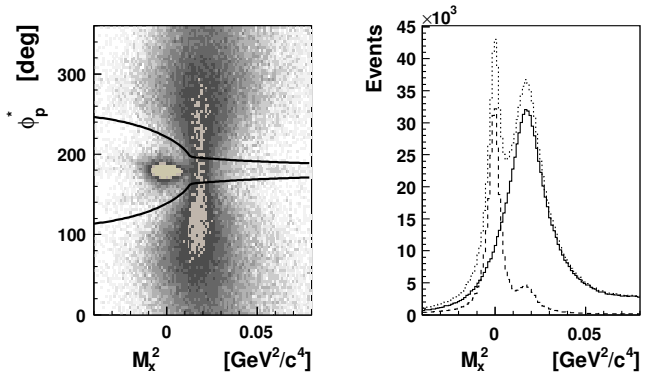

FIG. 1: The Bethe–Heitler rejection. Left: ϕ_p^* vs M_x^2 for $W = 1.25$ GeV/c^2. The cuts defined to reject the BH events are shown as solid curves and depend on W. Right: the resulting M_x^2 distribution in the W region considered. The dotted line shows the M_x^2 distribution prior to the cut, the solid line is what remains after the cut, and the dashed line represents the events eliminated by the cut.

nal in the Čerenkov detector. The $p\pi^0$ final state was identified using a cut on the reconstructed missing mass (M_x^2) of the detected electron and proton. Figure 1 (left) shows the center-of-mass azimuthal angle of the proton ϕ_p^* versus M_x^2. The most prominent feature is the Bethe–Heitler radiative tail (BH) associated with elastic scattering. Since the BH events peak at $M_x^2 = 0$ and lie primarily in the electron scattering plane, they were suppressed by suitable cuts in the M_x^2 - ϕ_p^* plane. Figure 1 (right) shows the effects of the cuts on the M_x^2 distribution.

A Monte Carlo simulation based on GEANT3 [9] was used to determine the acceptance of CLAS and to evaluate the efficiency of the BH cuts. Inelastic radiative losses were corrected for using the program EXCLURAD [10], which provides a covariant treatment of both hard and soft photon radiation in exclusive electroproduction and does not rely on the peaking approximation.

Differential cross sections were obtained at 9000 kinematic points, binned as follows: 15 bins in W, 5 bins in Q^2, 10 bins in $\cos\theta_\pi^*$, and 12 bins in ϕ_π^*. Cross sections are quoted at the center of each kinematic bin, and a correction was calculated to take into account non-linear dependencies of the cross section inside each bin. Systematic errors were estimated by varying the kinematic cuts, such as M_x^2, detector acceptance, particle identification and vertex reconstruction. Estimated uncertainties in the radiative and bin averaging corrections arising from their model dependence are also included. Figure 2 shows an example of the extracted cross sections as a function of ϕ_π^* for different $\cos\theta_\pi^*$ bins at $W = 1.25$ GeV/c^2 and $Q^2 = 4.2$ GeV^2/c^2.

In order to extract the Δ multipoles M_{1+}, E_{1+} and S_{1+}, the truncated multipoles expansion (TME) was commonly used at low Q^2. In the TME, the structure functions are expanded up to p- or d-waves in Legendre polynomials, whose coefficients are related to the multipoles [11]. The magnetic dipole transition $|M_{1+}|^2$ is then assumed to dominate the π^0 production at the Δ pole, and only the terms interfering with M_{1+} are retained. As the Δ resonance contribution to the cross section diminishes smoothly with increasing Q^2 [12], the TME becomes less accurate because M_{1+} dominance is no longer assured. Therefore, models that isolate the Δ amplitudes from the underlying backgrounds must be used.

The predominantly used approaches have been based on the effective Lagrangian expansions, which model the reactions in terms of meson and baryon degrees of freedom. MAID [13], which is commonly used to characterize resonance amplitudes, is an isobar model approach for photo- and electroproduction data. Other elaborations of the effective Lagrangian are the Dynamical [14], and DMT [15] models, which couple the baryon core and the pion cloud. SAID [16] is another approach often used to extract amplitudes from global data.

For the present case, the unitary isobar model (UIM) [7], developed at JLab, was used. This model incorporates the isobar approach as in Ref. [13]. The non-resonant background consists of the Born term and

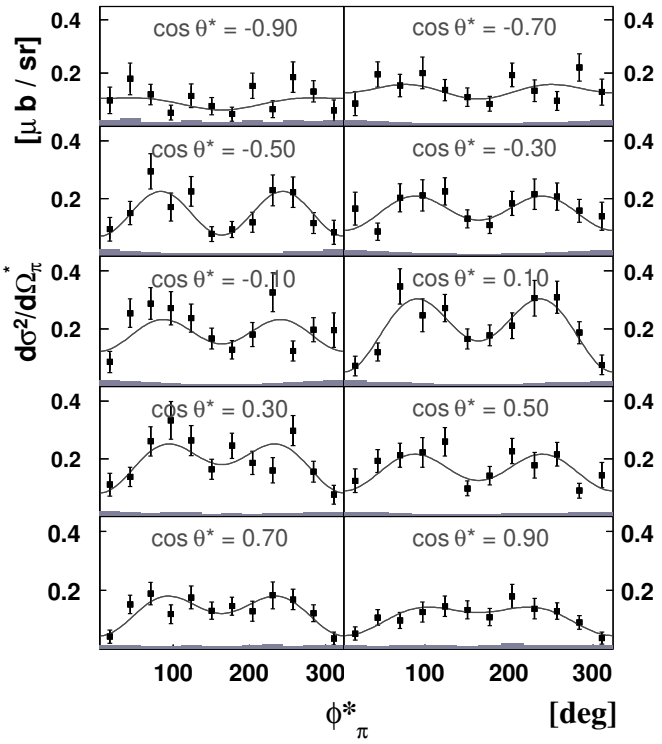

FIG. 2: The extracted virtual photon cross section as a function of ϕ_π^* for each $\cos(\theta_\pi^*)$ bin in the center-of-mass system at $W = 1.25$ GeV/c^2 and $Q^2 = 4.2$ GeV^2/c^2. The error bars are statistical, and the gray band at the bottom of each panel corresponds to the systematic. The solid curves represent the fit using UIM [7]. The fit was carried out utilizing 9000 such data points. Each Q^2 point was fitted separately.

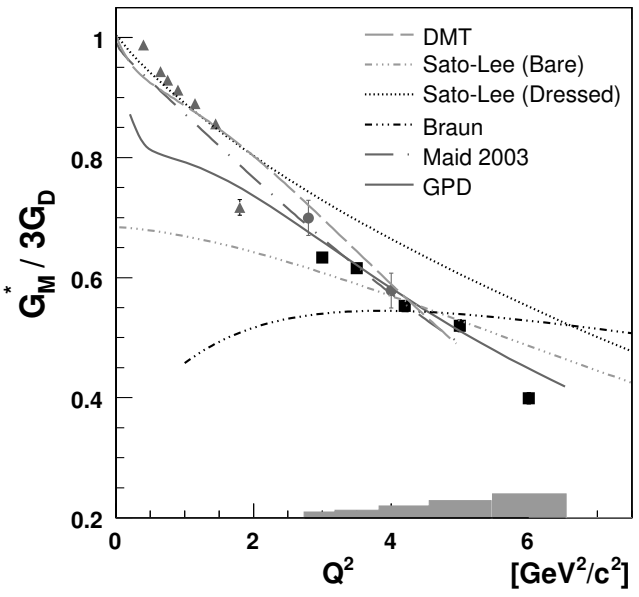

FIG. 3: The form factor $G_M^*/3G_D$. The filled squares are from the current CLAS experiment utilizing the UIM [7]. The errors shown are statistical, while estimated systematic errors are shown as gray bars at the bottom of the graph. Also shown are selected earlier published results. The filled triangles correspond to a recent analysis of previous CLAS data [17, 18], and the filled circles are from an earlier JLab Hall C experiment [15, 19]. The curves are due to the following calculations. Dashed: dynamical model of Ref [15]. Grey dot-dot-dash: dynamical model of Ref. [14] for the "bare" Δ (without the pion cloud). Black dotted: full dynamical model of Ref. [14]. Black dot-dot-dash: Light cone sum rule model of Ref. [20]. Dot-dash: MAID-2003 [13]. Grey solid: GPD model of Ref [21].

the t-channel ρ and ω contributions. To calculate the Born term the latest available measurements of the nucleon and pion form factors are used. Underlying tails from resonances such as the $P_{11}(1440)$, $D_{15}(1520)$ and $S_{11}(1535)$, which are modeled as Breit–Wigner shapes, are also incorporated. The total amplitude is unitarized using the K-matrix approach. The dependence of the extracted results on uncertainties in non-resonant and higher resonances contributions is included in the systematic errors. The results of the fit are given in Table I.

Figure 3 shows the extracted $G_M^*/3G_D$ as a function of Q^2 in the Jones–Scadron convention [2]. We used the $M_{1+} \leftrightarrow G_M^*$ conversion factor

$$G_M^* = \frac{M_N}{\hbar c k_\gamma}\sqrt{\frac{8 p_\pi \Gamma_\Delta}{3\alpha}\left(1+\frac{Q^2}{(M_\Delta+M_N)^2}\right)}M_{1+}(M_\Delta),$$

where k_γ and p_π are the center-of-mass momenta of the virtual photon and pion respectively, $M_\Delta = 1.23$ GeV/c^2, the resonance width Γ_Δ=120 MeV, and $G_D = (1+Q^2/0.71)^{-2}$. Also shown are selected earlier published results. The most notable feature is that G_M^* continues to decrease with Q^2 faster than the elastic magnetic form factor. This is consistent with Ref. [22], which pointed out that, through the application of chiral symmetry, G_M^* can be directly related to the isovector part of the nucleon elastic form factors. This idea was applied in the framework of Generalized Parton Distributions (GPDs) by Ref. [21], and later by Ref. [23], to suggest that the falloff of G_M^* is related to the falloff of G_E^p [24] through their mutual isovector form factor.

A recent calculation uses the light-cone sum-rules (LCSR) [20]. In this approach, the form factor is effectively governed by the overlap of the initial and final QCD wave functions. As shown in Fig. 3, there is modest agreement with experiment for Q^2 greater than a few GeV^2/c^2.

Figure 4 shows the extracted ratios R_{EM} and R_{SM}. R_{EM} is small and negative over the entire Q^2 range, indicating strong helicity non-conservation. R_{SM} is negative and its magnitude increases as a function of Q^2. Our results suggest that the region of Q^2 where pQCD processes would be expected to be valid is higher than currently accessible. Adding to the controversy, Ref. [25] has suggested that pQCD can possibly be invoked without strict helicity conservation if orbital angular momentum flips are included into the perturbative reaction mechanism. The prediction for R_{SM} of Ref. [25] is shown in Fig. 4 (lower panel).

Progress is being made in describing the $\gamma^* p \to \Delta$ transition at low Q^2 using the methods of lattice QCD (LQCD), where calculations of the magnetic form factor of this transition are being carried out up to $Q^2 \sim 1.5$ GeV^2/c^2. The results appear encouraging [26], however, at the Q^2 values of the present experiment, the application of LQCD is not yet feasible.

Included in Figs. 3 and 4 are the results of calculations using effective Lagrangian based models whose ingredients were tuned to fit earlier data at lower Q^2. Until a reliable treatment in terms of QCD degrees of freedom becomes fully developed, these models give unique insights into the baryon structures and their manifesta-

Q^2 GeV^2/c^2	$100 \cdot G_M^*/3G_D$	R_{EM} (%)	R_{SM} (%)
3.0	$63.4 \pm 0.2 \pm 0.9$	$-1.61 \pm 0.39 \pm 0.22$	$-11.5 \pm 0.5 \pm 2.01$
3.5	$61.4 \pm 0.4 \pm 1.2$	$-1.07 \pm 0.47 \pm 0.10$	$-13.0 \pm 0.7 \pm 1.13$
4.2	$55.2 \pm 0.5 \pm 1.9$	$-3.15 \pm 0.70 \pm 0.20$	$-16.4 \pm 1.2 \pm 1.38$
5.0	$52.2 \pm 1.0 \pm 2.8$	$-3.23 \pm 1.51 \pm 0.33$	$-24.8 \pm 2.7 \pm 2.8$
6.0	$39.9 \pm 1.5 \pm 4.0$	$-3.84 \pm 2.69 \pm 1.40$	$-24.8 \pm 5.3 \pm 3.0$

TABLE I: Results for $G_M^*/3G_D$, R_{EM} and R_{SM}. The first of the quoted errors is statistical, and the second represents our calculation of the systematic uncertainties. The quoted form factor G_M^* is defined according to the Jones–Scadron convention of Ref. [2].

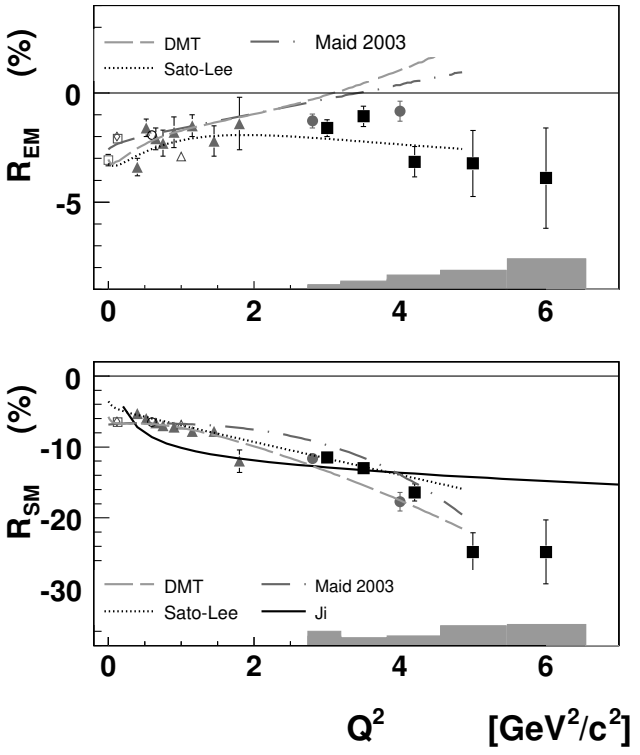

FIG. 4: The ratios R_{EM} (upper panel) and R_{SM} (lower panel). The filled red squares are from the UIM fit to the current CLAS experiment. The errors shown are statistical, while estimated systematic errors are shown as gray bars at the bottom of the graph. The filled triangles at lower Q^2 are the previously reported CLAS results [17]. The filled circles are from an earlier JLab Hall C experiment [15, 19]. The open triangles: JLab Hall-A [28]. Additional symbols at lower Q^2 are results of measurements by other laboratories as follows. Open squares: Bates [29]. Open trapezoids: Mainz [30]. The open circle: Bonn [31]. The curves are as follows. Dotted: full dynamical model of Ref. [14]. Dashed: dynamical model of Ref [15]. Dot-dash: MAID-2003 [13]. Solid: pQCD with orbital angular momentum effects of Ref [25].

tions in terms of the traditional hadronic degrees of freedom. A review of some of these models and the physical interpretations may be found in Ref. [27].

In summary, complete angular distributions for single π^0 electroproduction from protons are reported for a range of Q^2 from 3 to 6 GeV^2/c^2 and a range of W from π^0 threshold to 1.4 GeV/c^2. The quantities G_M^*, R_{EM}, and R_{SM} were extracted utilizing the isobar model [7]. The results indicate that the form factor G_M^* decreases with Q^2 faster than the elastic magnetic form factor. R_{EM} is small and negative, while R_{SM} remains negative and increases in magnitude. These results confirm the absence of pQCD scaling at these kinematics and suggest large helicity non-conservation. They provide strong constraints on isobar-based effective Lagrangian models, or on approaches employing fundamental partonic degrees of freedom such as LQCD, GPDs, LCSR and eventually pQCD. However, greater theoretical progress will be necessary before good quantitative agreement with the experimental high-Q^2 data is obtained.

We acknowledge the efforts of the staff of the Accelerator and the Physics Divisions at JLab that made this experiment possible. This work was supported by the U.S. Department of Energy, the National Science Foundation, the Italian Istituto Nazionale di Fisica Nucleare, the French Centre National de la Recherche Scientifique and the Commissariat à l'Energie Atomique, and the Korea Science and Engineering Foundation. The Southeastern Universities Research Association (SURA) operates the Thomas Jefferson National Accelerator Facility for the United States Department of Energy under contract DE-AC05-84ER40150.

* Current address:Massachusetts Institute of Technology, Cambridge, Massachusetts 02139-4307
† Current address:Physikalisches Institut der Universitaet Giessen, 35392 Giessen, Germany
‡ Current address:University of Massachusetts, Amherst, Massachusetts 01003
§ Deceased

[1] G.F. Chew, M.L. Goldberger, F.E. Low and Y. Nambu, Phys. Rev. **106**, 1345 (1957).
[2] H.F. Jones and M.D. Scadron, Annals Phys. **81**, 1 (1973).
[3] C. Becchi and G. Morpurgo, Phys. Lett. **17**, 352 (1965).
[4] N. Isgur, G. Karl and R. Koniuk, Phys. Rev. D **25**, 2394 (1982).
[5] S. Kamalov and S.N. Yang, Phys. Rev. Lett. **83**, 4494 (1999).
[6] A. J. Buchmann *et al.*, Phys. Rev. C **58**, 2478 (1998).
[7] I. Aznauryan , Phys. Rev. C **67**, 015209 (2003).
[8] B. Mecking *et al.*, Nucl. Inst. Meth. **A 503**, 513 (2003).
[9] GEANT - Detector description and simulation tool, CERN Program Library, Long Write-up W5013 , (1994).
[10] I. Afanasev, I. Akushevich, V.D. Burkert and K. Joo, Phys. Rev. D **66** 074004 (2002).
[11] A.S. Raskin and T.W. Donnelly, Annals Phys. **169**, 247 (1986).
[12] P. Stoler, Physics Reports **226**, 103 (1993).
[13] D. Drechsel, *et al.*, Nucl. Phys. **A 645**, 145 (1999).
[14] T. Sato and T. S. H. Lee, Phys. Rev. C **54**, 2660 (1996).
[15] S.S. Kamalov *et al.*, Phys. Rev. C **64**, 032201 (2001).
[16] R. Arndt *et al.*, Proc. of NSTAR2002, S. A. Dytman and E. S. Swanson, eds., World Scientific, Singapore, 234 (2002). Nucl-th/0301068.
[17] K. Joo, L.C. Smith *et al.*, Phys. Rev. Lett. **88**, 122001 (2002).
[18] I. G. Aznauryan, Private Communication (2006).
[19] V. V. Frolov *et al.*, Phys. Rev. Lett. **82**, 45 (1999).
[20] V.M. Braun *et al.* , Phys. Rev. D **73** 034020 (2006).
[21] Paul Stoler, Phys. Rev. Lett **91**, 172303 (2003).
[22] K. Goeke, M.V. Polyakov, and M. Vanderhaeghen, Prog. Part. Nucl. Phys. **47**, 401 (2001).
[23] M. Guidal *et al.*, Phys. Rev. D **72**, 054013 (2005).
[24] O. Gayou *et al.*, Phys. Rev. C **64**, 038202 (2001).

[25] X. Ji, J. P. Ma and F. Yuan, Phys. Rev. Lett. **90**, 241601 (2003).
[26] C. Alexandrou *et al.*, PoS LAT2005 **091**, hep-lat/0509140 (2005).
[27] V.Burkert and T.S.H. Lee, Int. J. Mod. Phys. **E 13**, 1035 (2004).
[28] J.J. Kelly *et al.*, Phys. Rev. Lett. **95**, 102001 (2005).
[29] C. Mertz *et al.*, Phys. Rev. Lett. **86**, 2963 (2001).
[30] R. Beck *et al.*, Phys. Rev. C **61**, 035204 (2000).
[31] R.W. Gothe *et al.*, Proc. of NSTAR2002, S. A. Dytman and E. S. Swanson, eds., World Scientific, Singapore, 220 (2002).